ARL-TR-9232 ● JULY 2021

DEVCOM ARMY RESEARCH LABORATORY

Modeling of Electrical Conductivity of Detonation Products in Octahydro-1,3,5,7-Tetranitro-1,3,5,7-Tetrazocine (HMX)

by Sergei Izvekov and Robert L Doney

NOTICES

Disclaimers

The findings in this report are not to be construed as an official Department of the Army position unless so designated by other authorized documents.

Citation of manufacturer's or trade names does not constitute an official endorsement or approval of the use thereof.

Destroy this report when it is no longer needed. Do not return it to the originator.

ARL-TR-9232 ● JULY 2021

Modeling of Electrical Conductivity of Detonation Products in Octahydro-1,3,5,7-Tetranitro-1,3,5,7-Tetrazocine (HMX)

Sergei Izvekov and Robert L Doney
Weapons and Materials Research Directorate,
DEVCOM Army Research Laboratory

REPORT DOCUMENTATION PAGE

Form Approved
OMB No. 0704-0188

1. REPORT DATE *(DD-MM-YYYY)*	2. REPORT TYPE	3. DATES COVERED (From - To)
July 2021	Technical Report	10 January 2020–30 September 2021

4. TITLE AND SUBTITLE
Modeling of Electrical Conductivity of Detonation Products in Octahydro-1,3,5,7-Tetranitro-1,3,5,7-Tetrazocine (HMX)

5a. CONTRACT NUMBER

5b. GRANT NUMBER

5c. PROGRAM ELEMENT NUMBER

6. AUTHOR(S)
Sergei Izvekov and Robert L Doney

5d. PROJECT NUMBER

5e. TASK NUMBER

5f. WORK UNIT NUMBER

7. PERFORMING ORGANIZATION NAME(S) AND ADDRESS(ES)
DEVCOM Army Research Laboratory
ATTN: FCDD-RLW-WA
Aberdeen Proving Ground, MD 21005-5069

8. PERFORMING ORGANIZATION REPORT NUMBER
ARL-TR-9232

9. SPONSORING/MONITORING AGENCY NAME(S) AND ADDRESS(ES)

10. SPONSOR/MONITOR'S ACRONYM(S)

11. SPONSOR/MONITOR'S REPORT NUMBER(S)

12. DISTRIBUTION/AVAILABILITY STATEMENT
Approved for public release: distribution unlimited.

13. SUPPLEMENTARY NOTES
ORCID ID(s): Sergei Izvekov, 0000-0003-4755-9138

14. ABSTRACT
In this report, modeling the electronic conductivity of low-temperature plasma formed from detonation products of the octahydro-1,3,5,7-tetranitro-1,3,5,7-tetrazocine (HMX) high explosive is performed using multi-term Boltzmann equation and Monte Carlo methods.

15. SUBJECT TERMS
electrical conductivity, plasma, octahydro-1,3,5,7-tetranitro-1,3,5,7-tetrazocine, HMX, Boltzmann kinetic equation, Monte Carlo

16. SECURITY CLASSIFICATION OF:			17. LIMITATION OF ABSTRACT	18. NUMBER OF PAGES	19a. NAME OF RESPONSIBLE PERSON
a. REPORT	b. ABSTRACT	c. THIS PAGE			Sergei Izvekov
Unclassified	Unclassified	Unclassified	UU	33	19b. TELEPHONE NUMBER (Include area code) (410) 306-0720

Standard Form 298 (Rev. 8/98)
Prescribed by ANSI Std. Z39.18

Contents

List of Figures

List of Tables

Acknowledgments

The authors wish to thank Drs Brian Barnes and Betsy Rice of the US Army Combat Capabilities Development Command Army Research Laboratory for helpful comments.

This work was supported in part by a grant of computer time from the DOD High Performance Computing Modernization Program at the Navy and DEVCOM Army Research Laboratory DOD Supercomputing Resource Centers.

1. Introduction

The knowledge of accurate electrical conductivity (EC) properties in detonation products for condensed high explosive (HE) in a broad range of temperatures T and pressures P is of fundamental importance to a number of research areas relevant to existing and future research programs at the US Army Combat Capabilities Development Command Army Research Laboratory. One area of particular importance is to further enhance critical DEVCOM Army Research Laboratory multiphysics modeling tools and the requisite material models that require the knowledge of electronic transport in the plasmas formed by the detonation products of condensed HE. However, for the condensed HE of interest such as octahydro-1,3,5,7-tetranitro-1,3,5,7-tetrazocine (HMX), the available experimental measurements are limited to a few thermodynamic states. In the absence of reliable experimental data on the EC of HE detonation plasma, theoretical techniques can provide crucial insight.

A key parameter in the research of ionization in detonation products is the EC, which depends on the temperature, pressure, and composition of detonation products.[1] The electrical direct-current (DC) conductivity σ due to ionization occurring behind the fronts of gaseous detonation waves and shock waves in exothermic systems has received scant attention in comparison with the conductance and ionization phenomena that occur in flames. The main reason for the lack of accurate quantitative experimental data is attributable to the difficulties encountered in measuring them—owing to the extremely fast rates of reaction and extreme thermodynamic conditions that occur in combustion processes behind shock fronts.

The noticeable EC of detonation products of condensed HE have been shown in a number of experimental and theoretical works.[1–9] The EC of most HE appears to be on the order of 0.1 S/m, with the highest value being observed for trinitrotoluene (TNT).[1,2,4] The exact mechanism of induced EC behind shock waves formed upon condensed HE detonation is still debated, and several contending mechanisms put forward include thermal ionization[10,11] (this mechanism is dominant in gaseous detonation waves), chemical ionization,[12] contact conductivity,[2,13] and dissociation of molecules into ions.[8]

There is considerable evidence that electronic transport plays an important role in the EC. Particularly, it has been determined that the value of EC positively correlates to the extent of the reaction zone. In the nonequilibrium reaction zone, the ionization is typically 1 or 2 orders of magnitude in excess of the thermal equilibrium value observed downstream the reaction zone. This points to the

ionization as a dominant mechanism of the EC. For example, as for many other condensed HE, a typical EC $\sigma(\tau)$ versus the duration τ of the high conductivity zone for HMX[7,9] has a Rayleigh distribution shape—with a maximum of about 0.7 S/m, achieved in the reaction zone, which then decreases to 0.2 S/m at the Chapman–Jouguet (CJ) point. It then levels off into a long plateau-like tail at values of about 0.05–0.1 S/m.

It has been also demonstrated[7] that the high σ positively correlates with the equilibrium ionization levels that exist downstream of the reaction zone. In contrast to gaseous detonation, for condensed HE detonation, the temperature effects on the conductivity are relatively weak.[8] The EC in many HE detonation waves was linked to the dissociation of water.[14] (The water content in the detonation products of the CHNO explosives TNT, 1,3,5-trinitro-1,3,5-triazinane (RDX), pentaerythritol tetranitrate [PETN], HMX, and triaminotrinitrobenzene [TATB] is around 20%.) However for HMX, there is no significant correlation of water content with the conductivity and carbon is considered a major contributor to the EC.[7] Furthermore, the conductivity of post-detonation products clearly correlates with the carbon content and can be partially explained by the contact model.[2]

In Taylor,[15] the computational framework to calculate the EC of low-temperature plasma (LTP) was implemented, which is based on ab initio electronic structure methods and the Green–Kubo (GK) relation. That framework has been applied to HMX detonation products in this report. However, the DC conductivity, which corresponds to zero frequency, $\omega = 0$, cannot be directly computed using the GK expression and must be obtained by extrapolating the low-frequency GK values, $\sigma(\omega)$, to zero.

A powerful theoretical approach to obtain the DC conductivity σ is based on the Boltzmann kinetic theory of charged test particles (electron swarm) in a neutral gas in the presence of an electric field. In the Boltzmann kinetic theory, the electrons are represented by the one-electron phase space distribution function $f(\mathbf{r}, \mathbf{v}, t)$, where $\mathbf{r}$, $\mathbf{v}$ are electron position and velocity coordinates, and electron–atom interactions are treated as collisions. The two most popular approaches for obtaining electronic transport properties of the swarm, including σ, is through solving the Boltzmann kinetic equation[16,17] or using the Monte Carlo (MC) method.[18,19] In this report, we applied these methods to calculate the σ of HMX detonation products.

2. Computational Methods

We considered the plasma formed in the reaction zone to be an LTP, broadly defined as a plasma with electron energies of the order of the ionization potential

of atoms and molecules. In the LTP, the EC is due to electronic transport with a negligible contribution from the ionic conductivity. For HE and the conditions of interest, the gaseous detonation products are considered to be weakly ionized ($n << N$, where n is the number density of electrons and N is the number density of neutrals). The validity of this approximation is confirmed by the equation of state (EOS) and MC simulations, both of which are described in detail in this section. In a weakly ionized plasma, the collisionality of the plasma species is dominated by scattering from neutrals. Consequently, in the LTP at the kinetic theory level, the σ, which relates the ohmic electron current density **J**,

$$\mathbf{J} = \sigma \mathbf{E}, \tag{1}$$

to the applied electric field $\mathbf{E} = \mathbf{E}(\mathbf{r}, t)$, is determined by the distribution of free electrons and electron mobility μ:

$$\sigma = n\mu . \tag{2}$$

The mobility is related to the electron bulk drift velocity **W**, one of the most important electron swarm parameters (bulk transport coefficients and reaction rates),[16,20]

$$\mu = \frac{W}{E} , \tag{3}$$

where $W = |\mathbf{W}|$, $E = |\mathbf{E}|$. The theoretic electron swarm parameters can be obtained using kinetic treatments coupled with the *hydrodynamic conditions* for the free electrons reviewed in the next sections.

2.1 Kinetic Theory, Hydrodynamic Conditions, Cross Sections, and Connection to Experiment

Under hydrodynamic conditions,[16] the phase space distribution function $f(\mathbf{r}, \mathbf{v}, t)$ may be expanded with respect to the gradients of the electron density $n(\mathbf{r}, t)$:

$$f(\mathbf{r},\mathbf{v},t) = f^{(0)}(\mathbf{v}) n(\mathbf{r},t) - \boldsymbol{f}^{(1)}(\mathbf{v}) \cdot \nabla n(\mathbf{r},t) + \hat{f}^{(2)}(\mathbf{v}) : \nabla\nabla n(\mathbf{r},t) . \tag{4}$$

Similarly, the flux $\boldsymbol{\Gamma}(\mathbf{r},t) = \mathbf{v} n(\mathbf{r},t)$ and source term $S(\mathbf{r}, t)$ in the continuity equation

$$\partial n(\mathbf{r},t)/\partial t + \nabla \cdot \boldsymbol{\Gamma}(\mathbf{r},t) = S(\mathbf{r},t) \tag{5}$$

can be expanded into density gradients (truncated at the orders $k = 1$ and $k = 2$, respectively)

$$\boldsymbol{\Gamma}(\mathbf{r},t) = \mathbf{W}_F n(\mathbf{r},t) - \hat{D}_F \cdot \nabla n(\mathbf{r},t) , \tag{6}$$

$$S(\mathbf{r},t) = S^{(0)} n(\mathbf{r},t) - \boldsymbol{S}^{(1)} \cdot \nabla n(\mathbf{r},t) + \hat{S}^{(2)} : \nabla\nabla n(\mathbf{r},t) \ , \tag{7}$$

where $\mathbf{W}_F$ is flux velocity vector and $\hat{D}_F$ is the diffusion tensor, which has rank 2. The resulting expansion of the continuity equation is the generalized diffusion equation

$$\frac{\partial n(\mathbf{r},t)}{\partial t} + \mathbf{W} \cdot \nabla n(\mathbf{r},t) - \hat{D} : \nabla\nabla n(\mathbf{r},t) = R_a n(\mathbf{r},t) \ , \tag{8}$$

where the coefficients are the *bulk* transport coefficients

$$R_a = S^{(0)} \quad \text{(net ionization frequency)}, \tag{9}$$

$$\mathbf{W} = \mathbf{W}_F + \boldsymbol{S}^{(1)} \quad \text{(bulk drift velocity)}, \tag{10}$$

$$\hat{D} = \hat{D}_F + \hat{S}^{(2)} \quad \text{(bulk diffusion tensor)}. \tag{11}$$

These transport coefficients are associated with the swarm's center-of-mass (COM) transport.[16] The explicit influence of nonconservative collisional processes on the swarm's COM transport is described by the correction terms $\boldsymbol{S}^{(1)}$ and $\hat{S}^{(2)}$. Obviously, in the absence of nonconservative processes, these two sets of transport coefficients coincide.

By far, the most widely used kinetic treatments are based on solving the two-term[21,22] or multi-term Boltzmann equation (MT-BE)[17,23] and the MC[18,19,24,25] simulation method reviewed in the next section. Both MT-BE and MC treat interactions of electrons with neutrals as the collision processes described by the differential cross section $\sigma_{S,k}(\varepsilon)$, where S denotes a type of neutral species and k denotes a type of collision (elastic, inelastic, and attachment). For this study, only isotropic scattering, when $\sigma_{S,k}$ become functions of electron kinetic energy ε, is accounted for. The elastic collisions utilize the conservative momentum transfer cross section $\sigma_{S,m}$, and similarly the inelastic collisions lead either to excitations or ionizations with the process cross sections given by (respectively) $\sigma_{S,exc}$ and $\sigma_{S,ioniz}$. The attachment reaction is described by $\sigma_{S,att}$. The total number of cross sections $\sigma_{S,k}$ is denoted by K_{tot}. The accuracy of experimentally derived cross sections is subject to the accuracy of the simulation methodology in which they were derived.

The most common way to develop cross sections is via an iterative process of tuning cross sections to match the two-term BE model swarm parameters to experimental reference data. Such cross sections may feature artificial accuracy with a reference two-term model, while more advanced kinetic models yield less-accurate results. Hence, the selection of cross sections for MT-BE and MC models

often requires additional validations.[26] The major source of the cross sections is the LXCat database.[27] LXCat is an open-access platform for curating data needed for modeling the electron and ion components of LTP. The data types presently supported by LXCat are scattering cross sections and swarm/transport parameters, ion-neutral interaction potentials, and optical oscillator strengths. Twenty-four databases, contributed by different groups around the world, can be accessed on LXCat.

There are three main experimental setups to determine electron swarm parameters: time of flight (ToF), steady-state Townsend (SST), and pulsed Townsend (PT) setups.[16,25,28,29] The bulk transport coefficients must be independent of the experimental setup from which they were obtained. Furthermore, the hydrodynamic conditions of Eq. 4 are well satisfied in all three experimental setups. If the SST conditions are reached, f becomes stationary and fully separable into velocity and space contributions, $f(\mathbf{r},\mathbf{v}) = f^{(0)}(\mathbf{v})n(\mathbf{r})$. The simulated setup used in the Boltzmann kinetic equation and MC calculations described in the next two sections corresponds to the ToF experiments in which the behavior of the electrons in an isolated electron swarm in free space with the electrodes not taken into consideration is studied.

In our calculations, we used ToF configurations to model electron transport. The MT-BE calculations utilized the MultiBolt computer code[17] and the MC simulations were carried out using the METHES collision code.[19] These codes are able to calculate swarm parameters associated with the ToF configuration. The MultiBolt framework can additionally handle the SST configuration.

2.2 Multi-term Boltzmann Equation

In this subsection, the basic framework of the hydrodynamic model is reviewed. This model is used to calculate swarm parameters observed in ToF experiments. These formulations are based on the transport theory comprehensively detailed by Kumar et al.[16] This framework is implemented in the MultiBolt code.

In the absence of a magnetic field, the MT-BE can be written as

$$\frac{\partial f}{\partial t} + \mathbf{v}\cdot\frac{\partial f}{\partial \mathbf{r}} + \frac{e}{m_e}\mathbf{E}\cdot\frac{\partial f}{\partial \mathbf{v}} = -C\left[f\right], \tag{12}$$

where e, m_e are charge and mass of the swarm particle (electron), which can be inhomogeneous and time dependent, and $-C[f]$ denotes the linear electron-neutral collision integral. Substituting Eq. 4 into Eq. 12, then solving for the coefficients of the kth density gradient, results in a system of equations for each distribution tensor function

$$\boldsymbol{a}_E \cdot \partial_v f^{(0)}(\mathbf{v}) - C\left[f^{(0)}(\mathbf{v})\right] = -R_a f^{(0)}(\mathbf{v}) \quad \text{for } k=0\ , \tag{13}$$

$$\boldsymbol{a}_E \cdot \partial_v \boldsymbol{f}^{(1)}(\mathbf{v}) - C\left[\boldsymbol{f}^{(1)}(\mathbf{v})\right] = \mathbf{v} f^{(0)}(\mathbf{v}) - R_a \boldsymbol{f}^{(1)}(\mathbf{v}) \text{ for } k=1\ , \tag{14}$$

$$\begin{aligned} &\boldsymbol{a}_E \cdot \partial_v \hat{f}^{(2)}(\mathbf{v}) - C\left[\hat{f}^{(2)}(\mathbf{v})\right] = \\ &\mathbf{v} \otimes \boldsymbol{f}^{(1)}(\mathbf{v}) - R_a \hat{f}^{(2)}(\mathbf{v}) - \mathbf{W} \otimes \boldsymbol{f}^{(1)}(\mathbf{v}) - \hat{D} f^{(0)}(\mathbf{v}) \text{ for } k=2\ , \end{aligned} \tag{15}$$

where $\otimes$ is the outer product, $\boldsymbol{a}_E = e\mathbf{E}/m_e$, and the distribution function is normalized by the following, $\int f^{(0)}(\mathbf{v})d\mathbf{v} = 1$, $\int \boldsymbol{f}^{(1)}(\mathbf{v})d\mathbf{v} = \int \hat{f}^{(2)}(\mathbf{v})d\mathbf{v} = 0$. Assuming that the electrical field **E** is uniform and *z*-directed, the bulk drift velocity **W** has only one component, W_z, in the *z*-direction, and the diffusion tensor $\hat{D}$ is taken to be symmetric with a transverse component, D_T, and longitudinal component D_L, with respect to the *z*-direction. Eqs. 13, 14, and 15 lead to the following expressions for transport coefficients:

$$R_a = \int C\left[f^{(0)}(\mathbf{v})\right]d\mathbf{v}\ , \tag{16}$$

$$W_z = \int v_z f^{(0)}(\mathbf{v})d\mathbf{v} + \int C\left[f_z^{(1)}(\mathbf{v})\right]d\mathbf{v}\ , \tag{17}$$

$$ND_T = \int v_x f_x^{(1)}(\mathbf{v})d\mathbf{v} + \int C\left[f_x^{(2)}(\mathbf{v})\right]d\mathbf{v}\ , \tag{18}$$

$$ND_L = \int v_z f_z^{(1)}(\mathbf{v})d\mathbf{v} + \int C\left[f_z^{(2)}(\mathbf{v})\right]d\mathbf{v}\ , \tag{19}$$

where $v = |\mathbf{v}|$, $\mathbf{v} = (v_x, v_y, v_z)$. The terms containing the collision operator $C[\cdot]$ describe the source/sink contribution to the bulk transport. The flux contributions to the drift velocity and diffusion coefficients are then

$$W_{F,z} = \int v_z f^{(0)}(\mathbf{v})d\mathbf{v}\ , \tag{20}$$

$$ND_{T,F} = \int v_x f_x^{(1)}(\mathbf{v})d\mathbf{v}\ , \tag{21}$$

$$ND_{L,F} = \int v_z f_z^{(1)}(\mathbf{v})d\mathbf{v}\ . \tag{22}$$

A common strategy for solving the MT-BE is to expand the $f(\mathbf{v})$ into a truncated series of orthogonal functional bases (e.g., spherical harmonics, Legendre polynomials, and so on). The common choice are Legendre polynomials, $\{P_l(\cos\vartheta)\}_{l=0}^{N_l-1}$, where the $\cos\vartheta = v_z/v$. Expanding these functions in terms of Legendre polynomials results in a comparatively simple system of equations to be solved. For example, we have

$$f^{(0)}(\mathbf{v}) = \sum_{l=0}^{N_l-1} f_l^{(0)}(v) P_l(\cos\theta) \ . \tag{23}$$

Similar expansions can be written for $\boldsymbol{f}^{(1)}(\mathbf{v})$ and $\hat{f}^{(2)}(\mathbf{v})$. By substituting these expansions into Eqs. 13, 14, and 15, a set of N_l coupled differential equations can be derived[17,20] for $f_l^{(0)}(v)$, $\boldsymbol{f}_l^{(1)}(v)$, and $\hat{f}_l^{(2)}(v)$. In most cases, a relatively small number of Legendre polynomials ($N_l = 4-10$) is needed to achieve satisfactory convergence of the solution $f(\mathbf{v})$.

It is convenient to write down the equations for $f_l^{(0)}(\varepsilon)$, $\boldsymbol{f}_l^{(1)}(\varepsilon)$, and $\hat{f}_l^{(2)}(\varepsilon)$ using the electron energy $\varepsilon = mv^2/2$ as an independent variable instead of v.[17] The $f_0^{(0)}(\varepsilon)$ is the electron energy distribution function (EEDF), which is normalized as $\int \varepsilon^{1/2} f_0^{(0)}(\varepsilon) d\varepsilon = 1$. The mean electron energy is then

$$\langle \varepsilon \rangle = \int \varepsilon^{3/2} f_0^{(0)}(\varepsilon) d\varepsilon \ . \tag{24}$$

The collision integral $C[f]$ is the sum of terms describing collisions of different kinds. Derivations of each of the collision terms are described in detail in Loureiro and Amorim.[20] To solve the differential equations for $f_l^{(0)}(\varepsilon)$, $\boldsymbol{f}_l^{(1)}(\varepsilon)$, and $\hat{f}_l^{(2)}(\varepsilon)$, a finite-differential scheme is employed.

2.3 Monte Carlo Method

In the MC simulation, the swarm is represented by the set of N_e electrons (typically N_e is in the range $1\times10^5 - 1\times10^6$), which undergo collisions with background-neutral particles. The bulk transport coefficients (Eqs. 10 and 11) are determined by time-averaging the trajectories $\{\boldsymbol{r}_i(t)\}_{i=1}^{N_e}$ of the individual electrons in the swarm. The bulk drift velocity **W** and diffusion tensor $\hat{D}$ (the diagonal element D_{aa} is the diffusion in the direction a)

$$\mathbf{W} = \frac{d}{dt}\langle \mathbf{r} \rangle \ , \tag{25}$$

$$\hat{D} = \frac{1}{2}\frac{d}{dt}\langle \Delta\mathbf{r} \otimes \Delta\mathbf{r} \rangle \tag{26}$$

are obtained as the coefficients for a linear regression of the swarm's COM,

$$\langle \mathbf{r} \rangle = \frac{1}{t}\frac{1}{N_e}\sum_i \int_0^t \mathbf{r}_i(t') dt' , \tag{27}$$

and swarm's squared width, $\langle \Delta\mathbf{r} \otimes \Delta\mathbf{r} \rangle$, $\Delta\mathbf{r} = \mathbf{r} - \langle \mathbf{r} \rangle$, versus simulated time t. The reaction rates are defined by

$$R_a = -\alpha = \frac{d}{dt} \ln N_e \ . \tag{28}$$

The flux contributions to the bulk drift velocity $\mathbf{W}$ and the bulk diffusion $\hat{D}$ are

$$\mathbf{W}_F = \left\langle \frac{d\mathbf{r}}{dt} \right\rangle = \langle \mathbf{v} \rangle \ , \tag{29}$$

$$\hat{D}_F = \langle \mathbf{r} \cdot \mathbf{v} \rangle - \langle \mathbf{r} \rangle \cdot \langle \mathbf{v} \rangle \ . \tag{30}$$

In the MC method the electron-neutral collisions are simulated explicitly for individual electrons and the trajectories of the electron ensemble are generated. The electronic ensemble trajectories are used to calculated the ensemble averages of interest, including $\langle \mathbf{r} \rangle$, $\langle \Delta\mathbf{r} \otimes \Delta\mathbf{r} \rangle$, which are used to obtain the transport coefficients (Eqs. 25, 26, 29, and 30).

Here, we describe the MC method as implemented in the METHES computer program[19] used in the present work. The electron trajectories $\{\mathbf{r}_i(t)\}_{i=1}^{N_e}$ are sampled in accordance with

$$\begin{aligned} \mathbf{r}_i(t + \Delta t_c) &= \mathbf{r}_i(t) + \mathbf{v}_i(t) \Delta t_c - \frac{e}{2m_e} \Delta t_c^2 \mathbf{E} \ , \\ \mathbf{v}_i(t + \Delta t_c) &= \mathbf{v}_i(t) - \frac{e}{m_e} \Delta t_c \mathbf{E} \ , \ i = 1, N_e \quad , \end{aligned} \tag{31}$$

where Δt_c is the time until the next collision of the electron with the neutral. The Δt_c is calculated using the null-collision technique. In this technique, the trial collision frequency $\nu_{MC} > \max_{t,i}\left(\nu_{tot,i}(t)\right)$ (where $\nu_{tot,i}(t) = N\sigma_{tot}v_i(t)$ is the total collision frequency, $\sigma_{tot}(\varepsilon) = \sum_{S,k} f_S \sigma_{S,k}(\varepsilon)$ is the total cross section, $f_S = N_S/N$ is the partial fraction of *S*th species) is first selected and remains unchanged over the simulation. Then, the current free-flight time is calculated as $\Delta t_c = -\nu_{MC}^{-1} \ln p_c$, where p_c is a random variable uniformly distributed in [0,1].

After a period Δt_c of free motion, the decision has to be made which electron undergoes which type of collision. The decision is made by first constructing the $N_e \times K_{tot}$ matrix that contains the collision frequencies of all possible processes column-wise. Subsequently, the matrix is normalized with the collision frequency ν_{MC}, and the rows are summed up cumulatively to obtain the (column-wise)

monotonically increasing collision matrix $\hat{C}$ with the elements of the form $\hat{C}_{im} = N\nu_i\nu_{MC}^{-1}\sum_{S=1}^{S(m)}\sum_{k=1}^{k(S,m)} f_S\sigma_{S,k}$, where $S(m)$, $k(S,m)$ are known integer functions. More detail is provided by Rabie and Franck.[19]

Next, the vector $\{p_{c,i}\}_{i=1}^{N_e}$ of random numbers uniformly distributed in [0,1] is generated. For the ith electron, the *m*th collision process, which is described by the *m*th cross section in the set $\{\sigma_{S,k}\}$, is accepted as follows: if $p_{c,i} < \hat{C}_{i1}$ (i.e., $p_{c,i}$ is the smaller of every number in the *m*th line of $\hat{C}$), then the first (m = 1) collision process is accepted, and if $\hat{C}_{im-1} \le p_{c,i} < \hat{C}_{im}$ where $m > 1$, then the *m*th collision process is accepted. In the METHES code, the ionization and attachment are considered as only nonconservative collisions that may change the N_e.

Two types of MC simulations are implemented in the METHES code: nonconserving and conserving. In the nonconserving MC simulations, N_e is allowed to change, $N_e(t)$, due to the ionization and attachment processes. In contrast, the conserving MC simulations, N_e is kept constant through the simulation by random removal/addition of the electrons to compensate creation/loss of electrons in nonconservative scatterings. Determination of the reaction rates in Eq. 28 requires nonconserving MC simulations. The EEDF $f_0^{(0)}(\varepsilon)$, mean energy $\langle\varepsilon\rangle$, transport coefficients Eqs. 25 and 26, and reaction rates Eq. 28 are determined from the positions **r**, velocities **v**, and the numbers of reaction events, after the electrons reach the steady state. Additional details on the implementation of conservative and nonconservative collisions and on the data sampling used to calculate averages are given in Rabie and Franck.[19]

2.4 Plasma Composition and Electron Density

Application of the MT-BE and MC methods to HE detonation products requires knowledge of initial partial fractions of neutrals $\{f_S\}$ at the thermodynamic conditions of interest. These data can be obtained either from theoretical (e.g., ab initio or thermochemical EOS calculations) or experiment. The EC of plasma formed due to ionization of the neutrals is determined by the electron equilibrium density distribution $n(\mathbf{r})$ and the transport coefficients. In the hydrodynamic model, the solutions of MT-BE, $f_l^{(0)}(\varepsilon)$, $\boldsymbol{f}_l^{(1)}(\varepsilon)$, and $\hat{f}_l^{(2)}(\varepsilon)$, are used to obtain only transport coefficients and finding n requires integrating the continuity equation Eq. 5 independently. In the nonconserving MC, $n(\mathbf{r},t)$ is mapped out from the electron trajectories $\{\mathbf{r}_i(t)\}_{i=1}^{N_e}$ as it converges to the equilibrium distribution n in the steady state. In general, the uniform equilibrium n can be

obtained independently, using free-energy calculations with the available plasma generalized chemical models (GCMs).[30] In the GCM treatments, the model free energy of the plasma is minimized with respect to the concentrations of the ions, neutrals, and n. The GCM n can be then used with MT-BE or MC electron swarm parameters to calculate σ. This approach is beneficial since n is obtained consistently with chemical composition of the plasma.

For weakly ionized plasma, the degree of ionization can be also calculated using the Saha equation.[31] We determined the composition of the HMX detonation products at a given thermodynamic state point using the Cheetah 9.0 EOS methodology. The available methodology permits the calculation of the degree of ionization and hence evaluation of the homogenous concentration of free electrons n. We used n from the Cheetah 9.0 EOS to calculate EC using the transport coefficients determined from MT-BE calculations. The EC was then calculated using nonconservative MC simulations independently (n can be used as an initial concentration in the MC calculations, but it is not necessary) and the results were similar.

2.5 Calculation Setup

We used two simulation approaches, which correspond to the ToF experimental setup. In the first approach, the species composition $\{f_S\}$ of the detonation products was obtained from Manaa et al.[32] ($T = 3500$ K, $\rho = 1900$ kg/m^3, conditions roughly similar to the CJ detonation state) and the ideal gas EOS was used to relate N to pressure P and temperature T. In this setup, the composition $\{f_S\}$ was kept fixed across the studied thermodynamic states (P, T). In the second set of simulations, we used the thermochemical code Cheetah 9.0 EOS methodology[33] to calculate the composition $\{f_S\}$ and equilibrium concentration of free electrons n as functions of P, T. In these calculations, the composition $\{f_S\}$ was a function of (P, T). The advantage of the latter approach is the availability of n, necessary to calculate the conductivity using the electron swarm properties.

The cross sections for specific species in the HMX detonation plasma were obtained from the LXCat database.[27] The data sets are detailed in Table 1. In spite of some significant differences in the details of the individual cross sections, most of these data sets yield the swarm parameters in good agreement with the experiments.[26] Several cross sections are plotted in Fig. 1.

Table 1 Chemical composition of HMX detonation products at $T = 2500$ K, $P = 9$ GPa using the Cheetah 9.0 EOS methodology. The footnote next to species name references the LXCat cross section database.[27] The rest of the species (mole fraction of 0.0536) were modeled using only elastic cross sections of N_2.

Species	N_2[a]	H_2O[b]	CO_2[c]	CO[b]	CH_4[d]	NH_3[c]	H_2[a]
Mole fraction	0.3416	0.2647	0.1705	0.09814	0.01752	0.02558	5.230×10^{-3}

[a]Biagi-v8.97 database[34]
[b]Itikawa database[35, 36]
[c]Hayashi database[37]
[d]IST-Lisbon database[38]

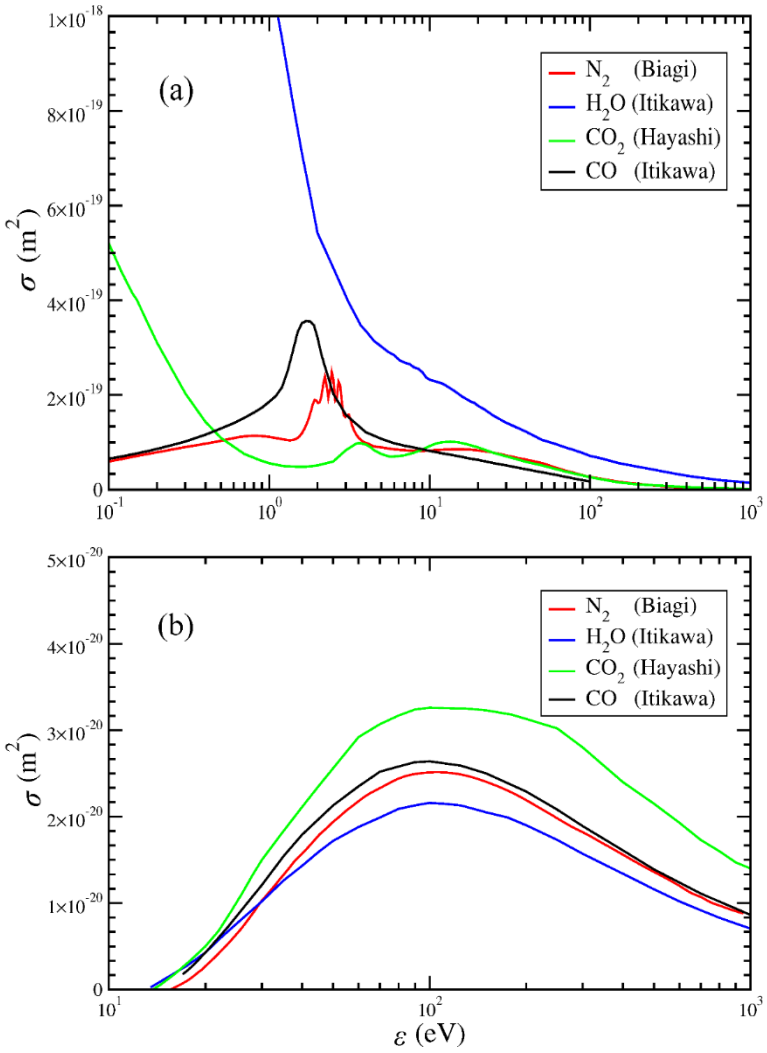

Fig. 1 a) Elastic-momentum transfer cross sections. b) Ionization cross sections.

2.6 LTP Transport Properties Using the MT-BE Hydrodynamic Model

The MT-BE model simulations model are based on the framework of the MultiBolt code.[17] In the MT-BE calculations, the size of the Legendre basis was chosen $N_l = 4$. The larger N_l does not lead to meaningful changes in the simulated plasma transport properties. The MT-BE EEDFs are displayed in Fig. 2. The EEDF is in good agreement with the EEDFs calculated using the MC METHES framework.[19] The distinct advantage of the MT-BE calculations is an absence of numerical noise clearly observed in the MC solution. The mean electron energy $\langle \varepsilon \rangle$ (Eq. 24) from the MT-BE model is shown in Fig. 3. The neutral density normalized first Townsend coefficient α/N is given in Fig. 4.

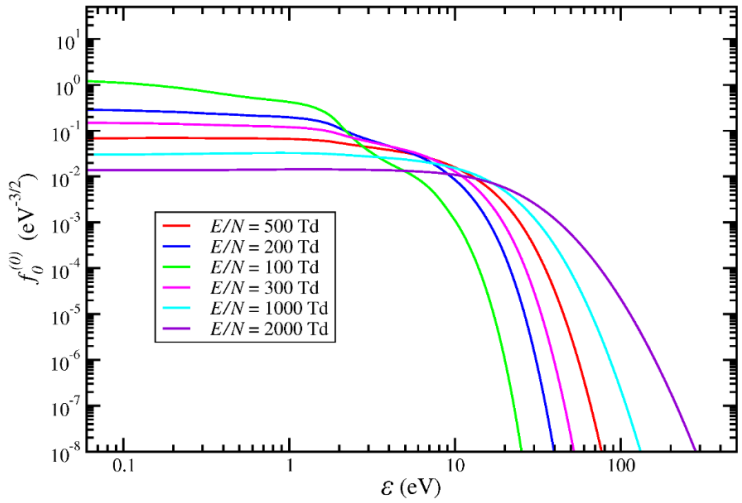

Fig. 2 EEDF $f_0^{(0)}(\varepsilon)$ for different values of reduced electric field *E/N* from the MT-BE model (chemical composition is in Table 1)

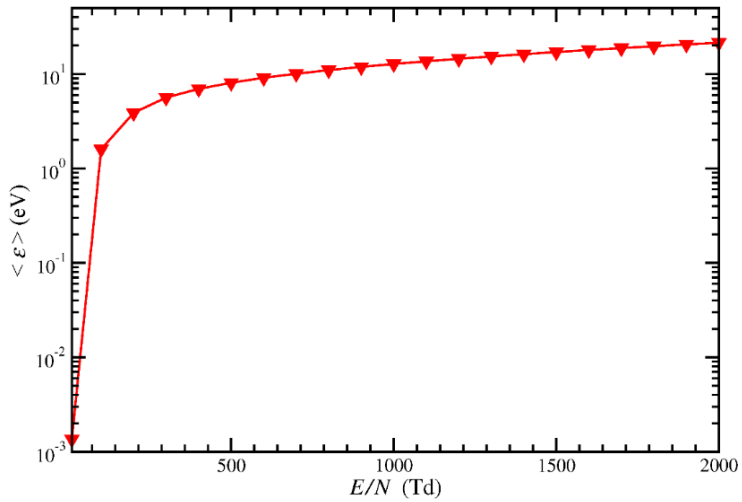

Fig. 3 Mean electron energy $< \varepsilon >$ vs. reduced electric field *E/N* from the MT-BE model

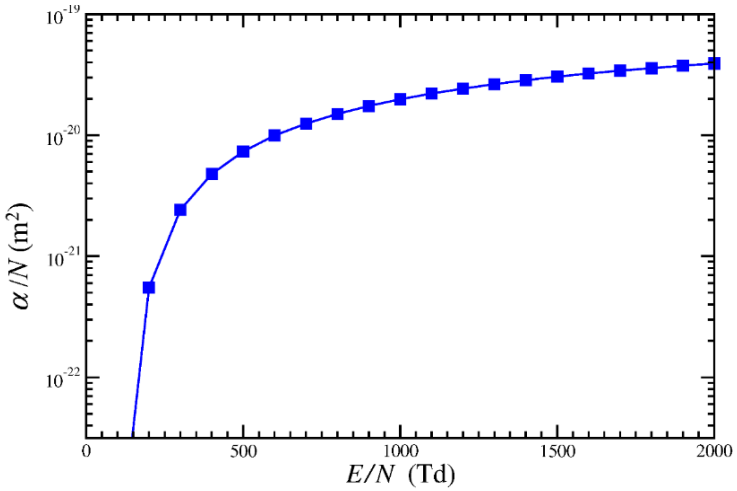

Fig. 4 Neutral density reduced first Townsend coefficient *α/N* vs. reduced electric field *E/N* from the MT-BE model

It is known that α/N for argon (Ar) using the cross section set of Biagi (in the present work, we used the Biagi cross section set for N_2, which is a dominant product) leads to very accurate data, agreeing with both the experimental data and the results using first principle B-spline R-matrix (BSR) cross sections,[17] with an error in E/N below a few percent. For Ar, the cross section set of Hayashi results in a less accurate α/N, yet still within only a few percent in E/N (In our calculations, we used the Hayashi cross section set for CO_2, another important species in the HMX detonation product plasma as shown in Table 1.) The bulk drift velocity $\mathbf{W}$, which has only one component W_z in the z-direction (Eq. 17), and its flux contribution $\mathbf{W}_F$ (Eqs. 10 and 20) are displayed in Fig. 5. For Ar, the Biagi cross section set notably outperforms the Hayashi and BSR sets at strong E/N fields (above 100 Td), generally yielding results within 10% of the available experimental data. The bulk longitudinal diffusion coefficient, neutral density product $D_L N$ versus E/N is given in Fig 6.

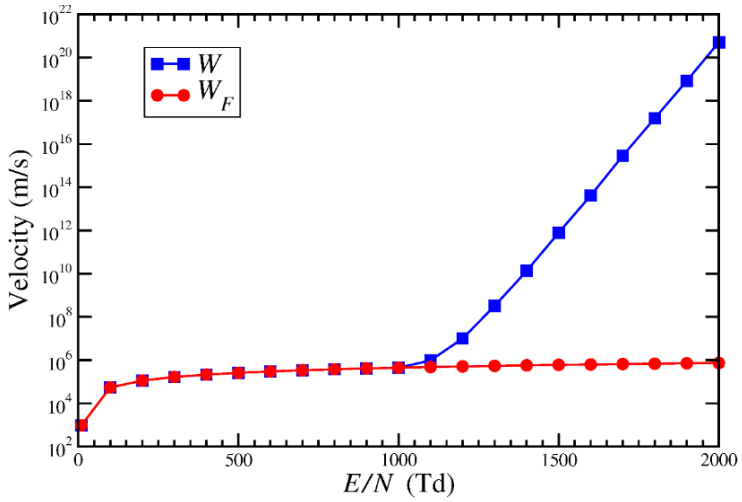

Fig. 5 Bulk drift velocity W and its flux contribution W_F vs. reduced electric field E/N from the MT-BE model

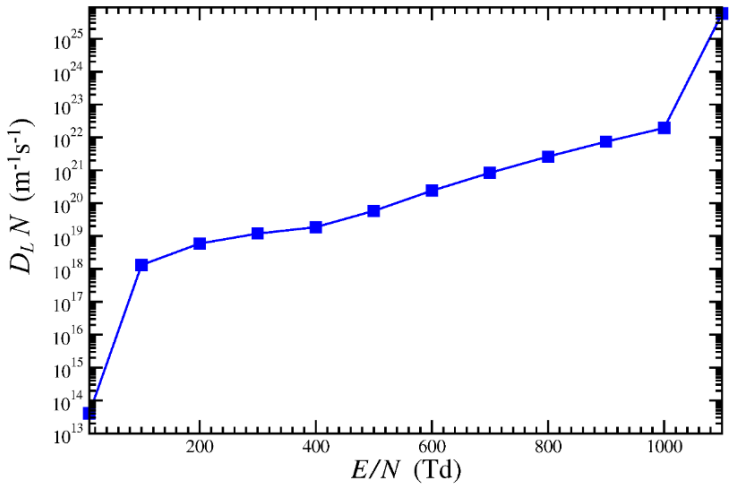

Fig. 6 Bulk longitudinal diffusion coefficient $D_L N$ vs. reduced electric field E/N from the MT-BE model

It is known that for Ar[17] up to 50 Td, the BSR and Biagi results are in excellent agreement with each other and experimental data. In this range, the Hayashi data deviates slightly from the BSR, Biagi, and experimental data with a difference of roughly 5%. The Biagi and Hayashi data better reproduce the experimental data at higher E/N, with an error not exceeding a factor of two between the calculated and measured data. We might expect a similar performance for systems studied here.

2.7 Electron Swarm Parameters Using the Monte Carlo Method

The electron transport coefficients were calculated using the MC simulations (Figs. 7 and 8). The calculations were carried out for the same two setups used in

the MT-BE calculations: the fixed composition $\{f_S\}$ with the ideal gas EOS and the composition $\{f_S\}$ using Cheetah 9.0 EOS method. We carried out two types of MC simulations: nonconserving, in which the total number electrons was allowed to change, $N_e(t)$, and conserving, in which the N_e was kept fixed at the initial value.

The nonconserving and conserving calculations produced identical swarm properties and EEDFs. The nonconserving MC simulations can be used to directly compute the EC if n is not available. In such direct calculations, n can be calculated as $n = \lim_{t\to\infty} N_{e,\sigma}(t)/V_\sigma$, where V_σ is a volume occupied by a sphere of radius R_σ equal to the current swarm width (Fig. 8a,b). ToF (or hydrodynamic) equilibrium is said to be reached when the $\mathbf{W}$, $\hat{D}$ (Eqs. 25 and 26) have become time independent; according to Kumar,[16] all the ToF transport coefficients relax to equilibrium on the same timescale T_{SST} and the swarm is considered in a steady state.[39] The $n(t) = N_{e,\sigma}(t)/V_\sigma$ typically converges at around $t > T_{SST}$. The $n(t)$ converges faster if the initial distribution $n(r,0)$ of the N_e electrons is Gaussian, similar to ToF experiments,[28] and with the half-width set to be equal to the R_σ that results in the n from the Cheetah 9.0 EOS.

The output from the nonconservative MC simulations for a composition shown in Table 1 and at two values of electric field strength, $E/N = 5$, 50 Td, is displayed in Figs. 7 and 8. Plots on the left are for $E/N = 5$ Td and the plots on the right are $E/N = 50$ Td. Shown are snapshot of electron swarm in space (Fig. 7a,b), $\langle\varepsilon\rangle$ is mean energy as a function of time t ($T_{SST} = t_0$ is the starting time the swarm is considered to be in steady state and the swarm data is being collected) (Fig. 7c,d); and swarm width $\sigma^2 \equiv \langle \Delta\mathbf{r}^2 \rangle$ in x-, y- and z-directions as functions of time t (slopes of these curves are, respectively, $2D_{xx}$, $2D_{yy}$, $2D_{zz}$, where $D_L = D_{zz}$, Eq. 26) (Fig. 8a,b); $\langle\mathbf{r}\rangle = (\langle x\rangle, \langle y\rangle, \langle z\rangle)$, which is a location of swarm COM (slopes of these curves are, respectively, $(W_x, W_y, W_z) = \mathbf{W}$, Eq. 25) (Fig. 8c,d). The initial number of electrons has been set to $N_e(0) = 10^5$. The energy and position of the initial electrons have been set to zero. The steady state is achieved within $T_{SST} =$ 0.5-1 ps of the simulation as labeled in Figs. 7 and 8. The transport properties from ME-BE and MC simulations were close; however, the MC simulations are computationally much more demanding to achieve a comparable convergence of the transport properties of the electron swarm.

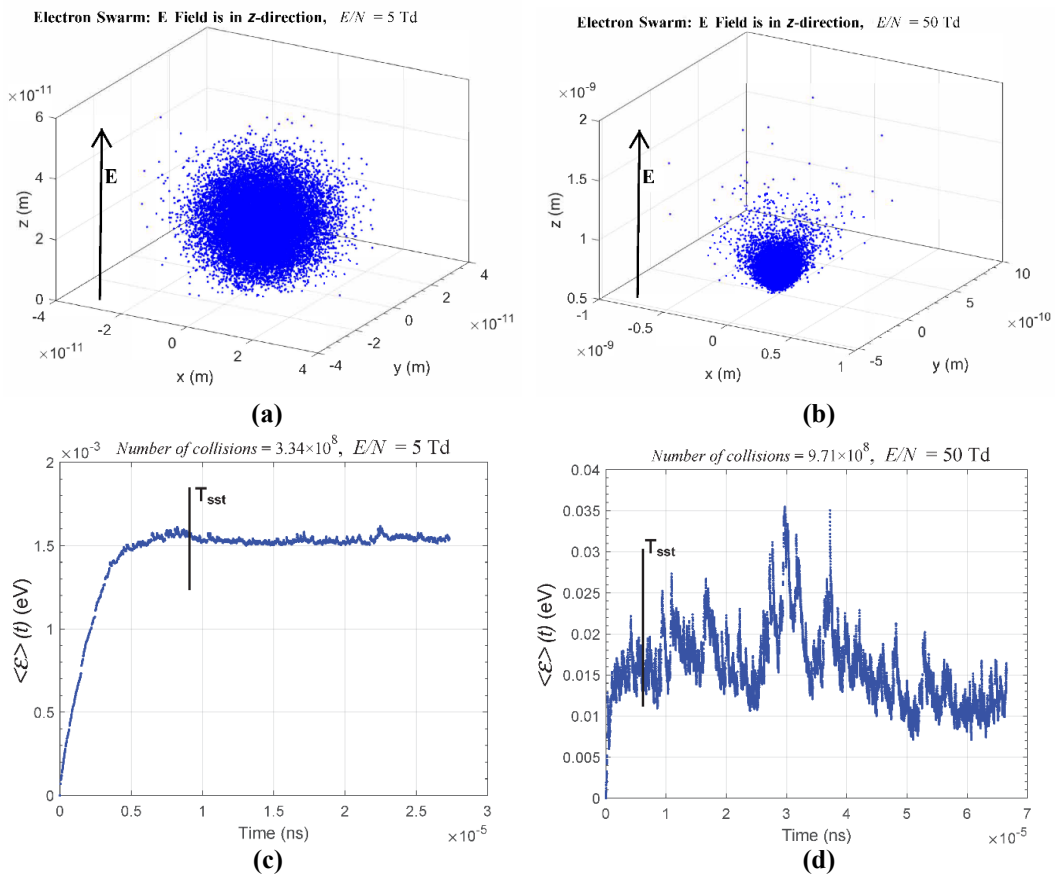

Fig. 7 The MC simulation (METHES code) showing selected electron swarm properties of HMX detonation products (T = 2500 K, P = 9 GPa) (part 1)

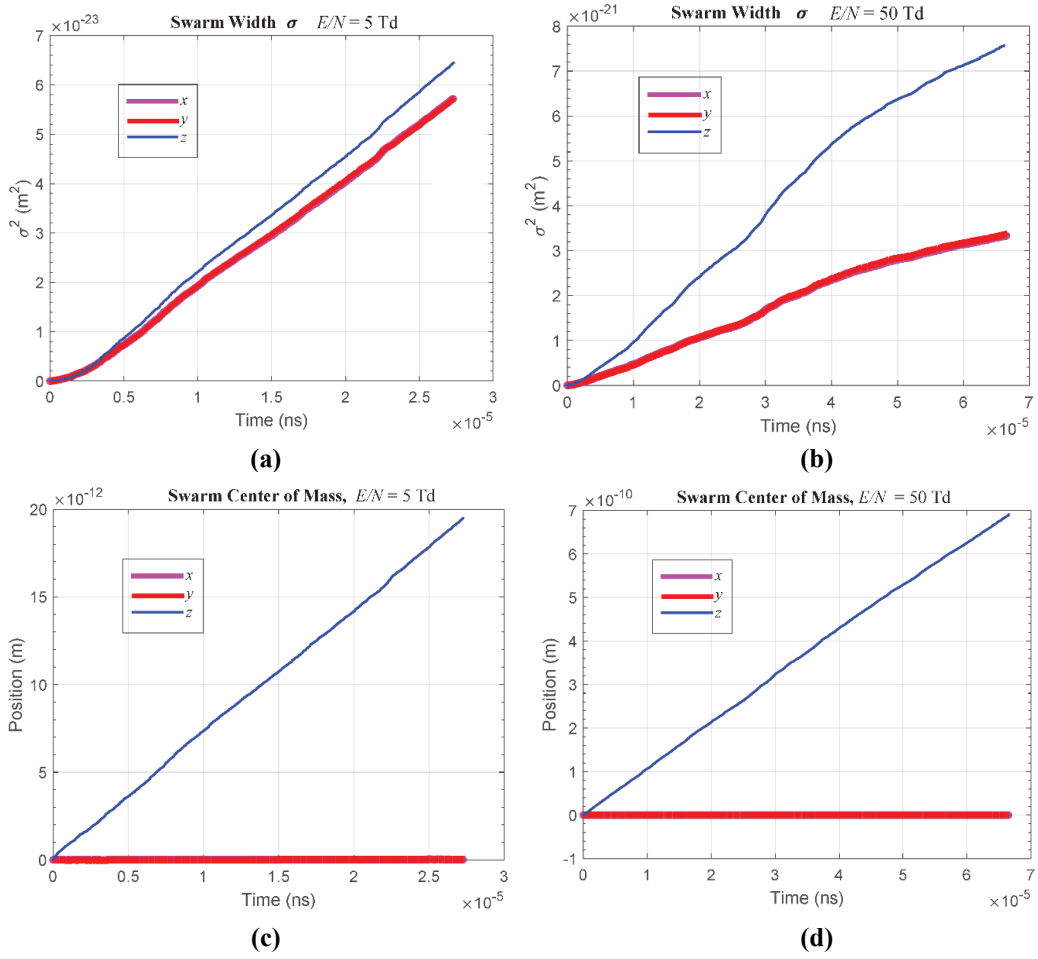

Fig. 8 The MC simulation (METHES code) showing selected electron swarm properties of HMX detonation products (T = 2500 K, P = 9 GPa) (part 2)

2.8 Electron Conductivity

We now connect the aforementioned calculations to determine the EC of HE as a function of pressure and temperature. Recall that the EC was determined from Eq. 2. The required electron mobility μ was calculated from Eq. 3 using the bulk drift velocity W, the transport coefficient produced by the MT-BE (Eq. 17) and the MC (Eq. 25) simulations. The W versus E from the ME-BE calculations is shown in Fig. 5. The EC was calculated using the swarm transport properties at $E/N = 5$ Td at which W versus $E/N =$ is linear. The EC from ideal and Cheetah 9.0 EOS calculations differ significantly (up to factor of 6.0) due to the difference in the composition $\{f_S\}$ (which was fixed in the ideal EOS calculations) and different N along the $P-T$ curves. However, the EC from both calculations behaved similarly with the change in the thermodynamic state (P,T).

Conductivity from the Cheetah 9.0 EOS and n, computed using MC simulations, is shown in Fig. 9. For all pressures evaluated, we see a decrease in EC with temperature up to 10,000 K. At 10 GPa, the change is much less pronounced. These profiles are combined to present an EC surface in Fig. 10. Figure 10 (left) plots $\ln_{10}\sigma$ so that details for the full range of pressures is visible. These low EC details are lost in Fig. 10 (right), where the EC is plotted on a linear scale. The plots illustrate a general trend of increased EC for lower temperatures and higher pressure. The values of concentration of free electrons, n, from the Cheetah 9.0 EOS calculations were larger than the MC values by a factor of up to 2–3 (the EC was larger proportionally). This highlights uncertainties with determining the EC using MT-BE or MC calculations.

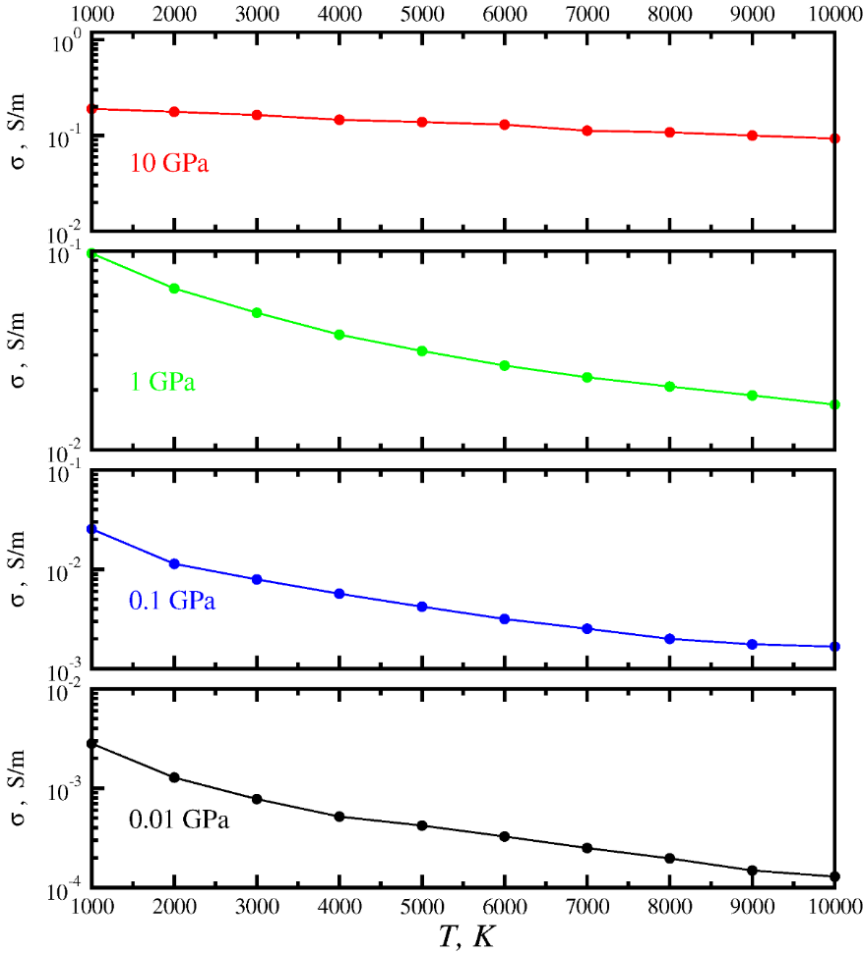

Fig. 9 The EC using Cheetah 9.0 EOS

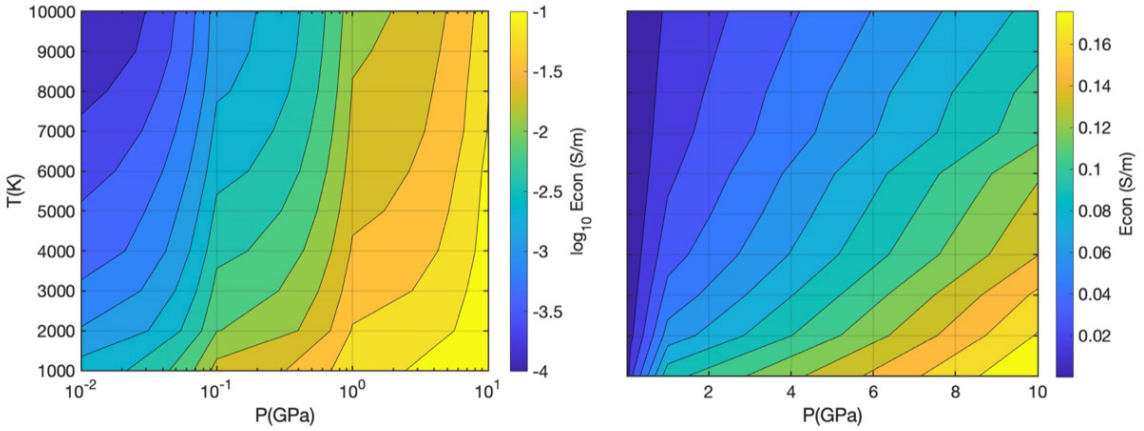

Fig. 10 Surfaces of EC σ : (left) $\log_{10}\sigma$ and (right) σ

3. Conclusion

We studied the electron transport properties of a LTP formed from HMX detonation products over a wide range of pressures and temperatures. The electronic transport properties were simulated in the frameworks of the MT-BE and MC methods. The MT-BE calculations employed the MultiBolt computer code program and the MC simulations were carried out using the METHES program. We considered the HMX detonation product EOS from the ideal gas assumption and Cheetah 9.0 thermochemical code calculations. Cheetah 9.0 was also used to evaluate the equilibrium concentration of free electrons. The MT-BE and MC simulations used the cross section sets available from the open-source LXCat database.

These results can be used to develop a functional form of $\sigma = \sigma(T, P)$, which can then be utilized by other modeling codes.

4. References

1. Cook MA. The science of high explosives. Reinhold Pub Corp; 1966.
2. Hayes B. Electrical measurements in reaction zones of high explosives. In: Proceedings of the 10th Symposium (Int.) on Combustion; 1965; Cambridge, UK. Combustion Inst. p. 869–874.
3. Tanaka K. Measurement of electrical conductivity in detonation products. In: Report on 5th International Colloquium on Gasdynamics of Explosions and Reactive Systems; 1975.
4. Ershov AP, Satonkina NP, Dibirov OA, Tsykin SV, Yanilkin YV. A study of the interaction between the components of heterogeneous explosives by the electrical-conductivity method. Combust Explos. 2000;36(5):639–649.
5. Gilev SD, Trubachev AM. Detonation properties and electrical conductivity of explosive-metal additive mixtures. Combust Explos. 2002;38(2):219–234.
6. Piehler T, Hummer C, Benjamin R, McNesby K, Summer E, Boyle V. Preliminary study of coupling electromagnetic energy to Primasheet-1000 explosive. Army Research Laboratory (US); 2013. Report No.: ARL-TR-6446.
7. Satonkina NP. Chemical composition of detonation products of condensed explosives and its relationship to electrical conductivity. J Phys Conf Ser. 2018;946:012059-7.
8. Satonkina N, Ershov A, Kashkarov A, Mikhaylov A, Pruuel E, Rubtsov I, Spirin I, Titova V. Electrical conductivity distribution in detonating benzotrifuroxane. Sci Rep. 2018;8:9635-7.
9. Satonkina NP. Influence of the grain size of high explosives on the duration of a high conductivity zone at the detonation. Sci Rep. 2019;9:12256-8.
10. Schulz JC, Gottiparthi KC, Menon S. Ionization in gaseous detonation waves. Shock Waves 2012;22(6):579–590.
11. Wang X, Ye D, Gu F. Research on the thermal ionization model of detonation products by quantum mechanics methods. Combust Explos. 2008;44(1):101–109.
12. Cavenor MC, Ubbelohd AR, Munday G. Chemi-ionization in detonation chemistry. Combust Flame. 1972;18(1):99–101.

13. Hayes B. On the electrical conductivity in detonation products. In: Proceedings of 4th Symposium (International) on Detonation. Office of Naval Research; 1967. p. 595–601.

14. Mitchell AC, Nellis WJ. Equation of state and electrical-conductivity of water and ammonia shocked to the 100 GPa (1 Mbar) pressure range. J Chem Phys. 1982;76(12):6273–6281.

15. Taylor DE. ECON-KG: a code for computation of electrical conductivity using density functional theory. Army Research Laboratory (US); 2017. Report No.: ARL-TR-8196.

16. Kumar K, Skullerud HR, Robson RE. Kinetic-theory of charged-particle swarms in neutral gases. Aust J Phys. 1980;33(2B):343–448.

17. Stephens, J. A multi-term Boltzmann equation benchmark of electron-argon cross-sections for use in low temperature plasma models. J Phys D-Appl Phys. 2018;51(12):125203–125211.

18. Lucas J, Saelee HT. A comparison of a Monte Carlo simulation and Boltzmann solution for electron swarm motion in gases. J Phys D-Appl Phys. 1975;8(6):640–650.

19. Rabie M, Franck CM. METHES: a Monte Carlo collision code for the simulation of electron transport in low temperature plasmas. Comput Phys Commun. 2016;203:268–277.

20. Loureiro J, Amorim Filho JD. Kinetics and spectroscopy of low temperature plasmas. Springer; 2016.

21. Lin SL, Robson RE, Mason EA. Moment theory of electron-drift and diffusion in neutral gases in an electrostatic-field. J Chem Phys. 1979;71(8):3483–3498.

22. White RD, Robson RE, Schmidt B, Morrison MA. Is the classical two-term approximation of electron kinetic theory satisfactory for swarms and plasmas? J Phys D-Appl Phys. 2003;36(24):3125–3131.

23. Petrovic ZL, Dujko S, Maric D, Malovic G, Nikitovic Z, Sasic O, Jovanovic J, Stojanovic V, Radmilovic-Radenovic M. Measurement and interpretation of swarm parameters and their application in plasma modelling. J Phys D-Appl Phys. 2009;42(19):33.

24. Thomas, RWL, Thomas WRL. Monte Carlo simulation of electrical discharges in gases. J Phys B: At Mol Phys. 1969;2(5):562.

25. Sakai Y, Sakamoto S, Tagashira H. Variation of steady-state electron mean energy between parallel plates in argon. J Phys B: At Mol Phys. 1972;5(5):1010–1016.

26. Pitchford LC, Alves LL, Bartschat K, Biagi SF, Bordage MC, Phelps AV, Ferreira CM, Hagelaar GJM, Morgan WL, Pancheshnyi S, Puech V, Stauffer A, Zatsarinny O. Comparisons of sets of electron-neutral scattering cross sections and swarm parameters in noble gases: I. Argon. J Phys D-Appl Phys. 2013;46(33):334001–19.

27. CDAP database. LXCat; c2020 [accessed 2020 July 10]. www.lxcat.net.

28. Robson RE. Transport phenomena in the presence of reactions: definition and measurement of transport coefficients. Aust J Phys. 1991;44(6):685–692.

29. Dujko S, White RD, Petrovic ZL. Monte Carlo studies of non-conservative electron transport in the steady-state Townsend experiment. J Phys D-Appl Phys. 2008;41(24):245205–11.

30. Redmer R. Physical properties of dense, low-temperature plasmas. Phys Rep.-Rev Sec Phys Lett. 1997;282(2-3):35–157.

31. Vandesanden MCM, Schram P, Peeters AG, Vandermullen JAM, Kroesen GMW. Thermodynamic generalization of the Saha equation for a 2-temperature plasma. Phys Rev A 1989;40(9):5273–5276.

32. Manaa MR, Fried LE, Melius CF, Elstner M, Frauenheim T. Decomposition of HMX at extreme conditions: a molecular dynamics simulation. J Phys Chem A 2002;106(39):9024–9029.

33. Fried L, Souers P. CHEETAH: a next generation thermochemical code. Lawrence Livermore National Laboratory; 1994. Report No.: UCRL-ID-117240.

34. Biagi SF. Monte Carlo simulation of electron drift and diffusion in counting gases under the influence of electric and magnetic fields. Nucl Instrum Methods Phys Res Sect A-Accel Spectrom Dect Assoc Equip. 1999;421(1-2):234–240.

35. Itikawa Y, Mason N. Cross sections for electron collisions with water molecules. J Phys Chem Ref Data 2005;34(1):1–22.

36. Itikawa Y. Cross sections for electron collisions with carbon monoxide. J Phys Chem Ref Data 2015;44(1):013105–17.

37. Hayashi M. Bibliography of electron and photon cross sections with atoms and molecules published in the 20th century - Argon. National Institute for Fusion Science of Japan; 2003. Report No.: NIFS-DATA--72. www.nifs.ac.jp/report/nifs-data072.html.

38. Alves LL. The IST-LISBON database on LXCat. J Phys Conf Ser. 2014;565(1):012007.

39. Boeuf JP, Marode E. Monte Carlo simulation of electron swarm motion in SF6. J Phys D-Appl Phys. 1984;17(6):1133–1148.

List of Symbols, Abbreviations, and Acronyms

Ar	argon
ARL	Army Research Laboratory
BE	Boltzmann equation
CH_4	methane
CJ	Chapman–Jouguet
CO	carbon monoxide
CO_2	carbon dioxide
COM	center-of-mass
DC	direct-current
EC	electronic conductivity
EEDF	electron energy distribution function
EOS	equation of state
GCM	generalized chemical model
GK	Green–Kubo
H	hydrogen
H_2O	water
HE	high explosive
HMX	octahydro-1,3,5,7-tetranitro-1,3,5,7-tetrazocine
LTP	low-temperature plasma
MC	Monte Carlo
METHES	MC collision code
MT-BE	multi-term Boltzmann equation
MultiBolt	MT-BE code
N	nitrogen
NH_3	ammonia
PETN	pentaerythritol tetranitrate
PT	pulsed Townsend
RDX	1,3,5-trinitro-1,3,5-triazinane
SST	steady-state Townsend
TATB	triaminotrinitrobenzene

TNT	trinitrotoluene
ToF	time of flight

1 (PDF)	DEFENSE TECHNICAL INFORMATION CTR DTIC OCA
1 (PDF)	DEVCOM ARL FCDD RLD DCI TECH LIB
2 (PDF)	DEVCOM ARL FCDD RLW WA S IZVYEKOV FCDD RLW TD R DONEY